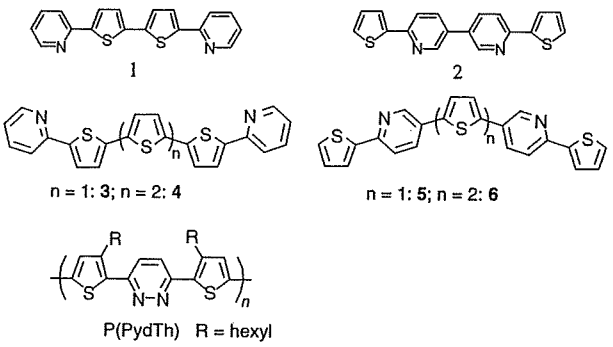

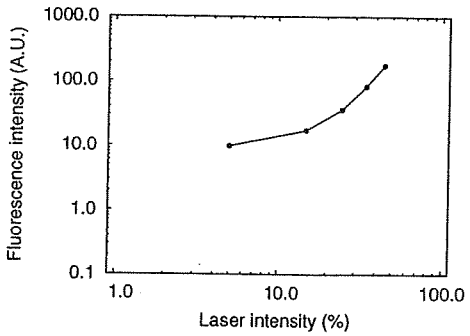

Fig. 2. Dependence of fluorescence intensity on the laser intensity at 780 nm. Data for the co-oligomer **1** in chloroform.

π-conjugation length did no show strong dependence of the fluorescence intensity on the laser intensity when the laser intensity is not strong (e.g., cf. data shown in Fig. 2 for the co-oligomer 1). This suggests that 1 and 2 were not so active for the two-photon excitation. The shorter π-conjugation system may not be suited for an effective two-photon excitation. However, when the laser intensity becomes stronger, the fluorescence shows nonlinear increase by increasing the laser intensity and the final slope of the curve seems to be larger than the average slopes in the figures in Figure 1. The reason for the larger slope in the region of the strong laser intensity and the small slope in the region of weaker laser intensity is not clear, however, the results suggest contribution of higher-order multi-photon absorption at strong laser intensity, and further detailed examination of the phenomenon is expected to reveal the origin of the nonlinear behavior.

As shown in Figure 1, co-oligomers **3**–**6** with a longer π-conjugation system and the intramolecular CT electronic structure show a strong linear relationship between the laser intensity and the fluorescence intensity in logarithm scales, indicating that they are active for the two-photon excitation. The intensity of the fluorescence increases roughly linearly with (laser intensity).[2] The copolymer P(PydTh) also shows a strong dependence of fluorescence on the laser intensity as shown in Figure 3.

The cross section (σ_{2PE}) of the two-photon absorption was determined for the co-oligomers **3**–**6** and P(PydTh) from the data exhibited in Figures 1 and 3, and the data are shown in Table I. The UV-vis peak positions (λ_{max}) and the cut-off positions of the co-oligomers and polymer are also shown in Table I. As shown in Table I, the co-oligomers **3**–**6** and P(PydTh) give larger σ_{2PE}'s than those of mSEGFP used as the standard. σ_{2PE} of α-Th_6 was also estimated under the same conditions as shown in Table I, and the estimated value is considerably smaller than those of the co-oliogmers **3**–**6**, although α-Th_6 has a π-conjugation length similar to those of the co-oligomers **3**–**6**. The much larger σ_{2PE}'s of the co-oligomers **3**–**6** than that of α-Th_6 suggest an important contribution of the CT electronic structure of the co-oligomers **3**–**6** to σ_{2PE}.

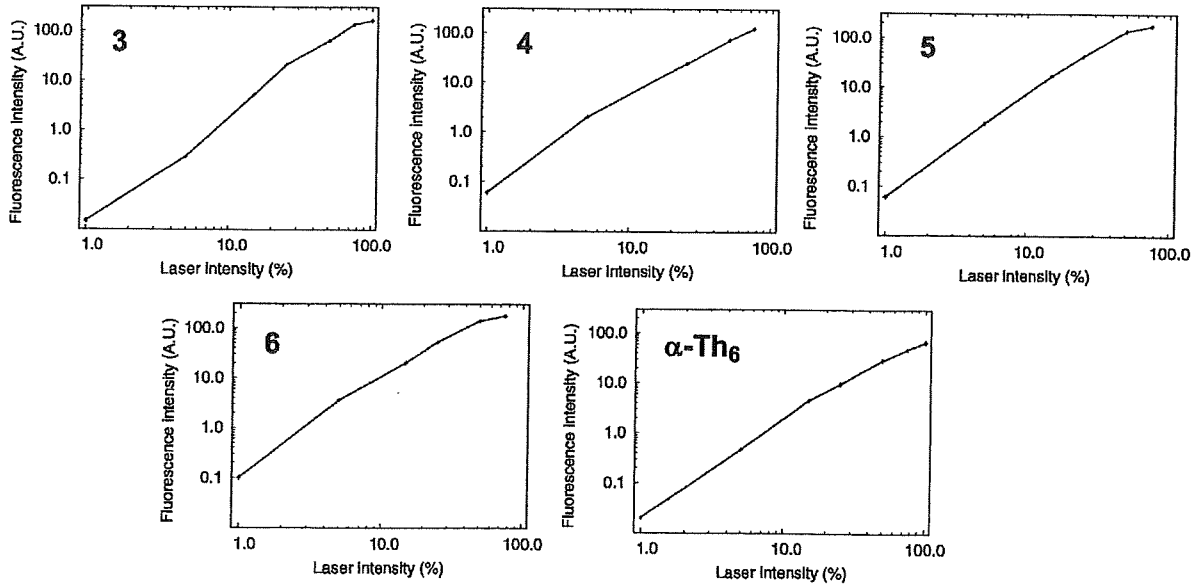

Fig. 1. Dependence of fluorescence intensity on the laser intensity at 780 nm. Data obtained with the co-oligomers **3**–**6** in dimethyl sulfoxide. Fluorescence intensity is given in an arbitrary unit.

COMMUNICATION

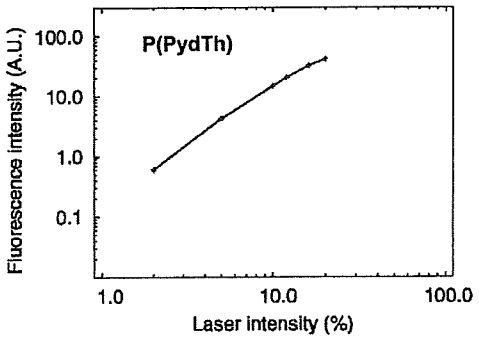

Fig. 3. Dependence of fluorescence intensity of P(PydTh) in xylene.

Table I. Fluorescence quantum yield, Φ, and cross section, σ_{2PE}, of the two-photon absorption of the co-oligomers **3–6** and copolymer P(PydTh).[a]

Sample	c (M)	Φ	σ_{2PE} at 780 nm (GM)	λ_{max} (nm)	Cut-off (nm)
mSEGFP	6.6×10^{-5}	0.6	10		
3	1.1×10^{-4}	0.21	24	418	475
4	0.7×10^{-4}	0.35	26	435	505
5	1.5×10^{-4}	0.33	23	384	470
6	2.8×10^{-4}	0.37	14	408	480
P(PydTh)	3.9×10^{-5}	0.59	23	449	530
α-Th_6	9.6×10^{-4}	0.3	1.1	432	520

[a]Concentration of P(PydTh) is based on the repeating unit of the copolymer.

P(PydTh) showed a σ_{2PE} value comparable to those of the co-oligomers **3–6**, suggesting that the π-conjugation length composed of 5 or 6 aromatic units was enough for the two-photon excitation by the CT-type compounds. The obtained results and further detailed studies based on the two-photon excitation behavior of π-conjugated molecules and polymers are expected to give better understanding of electronic state of the π-conjugated molecules and polymers.

Acknowledgments: We are grateful to Professor H. Fukumoto and Dr. T. Yasuda of Tokyo Institute of Technology and Dr. Tomoki Matsuda of Hokkaido University for their experimental supports. This research was partly supported by a Grant-in-Aid for Science Research in Priority Area "Super-Hierarchical Structures" and Special Education and Research Expenses for "Post-Silicon Materials and Devices Research Alliance" from the Ministry of Education, Culture, Sports, Science, and Technology, Japan.

References and Notes

1. M. Albota, D. Beljonne, J.-L. Brédas, J. E. Ehrlich, J.-Y. Fu, A. A. Heikal, S. E. Hess, T. Kogej, M. D. Levin, S. R. Marder, D. McCord-Maughon, J. W. Perry, H. Röckel, M. Rumi, G. Subramaniam, W. W. Web, X.-L. Wu, and C. Xu, *Science* 281, 1653 (**1998**).
2. B. Cumpston, S. P. Ananthavel, S. Barlow, D. L. Dyer, J. Ehrlich, L. L Erskine, A. A. Heikal, S. M. Kuebler, I.-Y. S. Lee, D. McCord-Maughon, J. Qin, H. Röckel, M. Rumi, X.-L. Wu, S. R. Marder, and J. W. Perry, *Nature* 398, 51 (**1999**).
3. F. Stabo-Eeg, M. Lindgren, P. R. Nilsson, O. Inganäs, and P. Hammarström, *Chem. Phys.* 336, 121 (**2007**).
4. M. Shimizu, M. Schelper, K. Mochida, T. Hiyama, M. Adachi, Y. Sasaki, S. Akiyama, S. Maeda, H. Kanbara, Y. Mori, and T. Kurihara, *Adv. Mater.* 19, 1826 (**2007**).
5. N. Pfeffer, P. Raimond, F. Charra, and J.-M. Nunzi, *Chem. Phys. Lett.* 201, 357 (**1993**).
6. H. Ohkita and S. Ito, *Kokagaku* 31, 84 (**2000**); *Chem. Abstr.* 135, 377757v (**2001**).
7. G. A. Blab, P. H. M. Lommerse, L. Cognet, G. S. Harms, and T. Schmidt, *Chem. Phys. Lett.* 350, 71 (**2001**).
8. K. Okamoto, T. Nagai, A. Miyawaki, and Y. Hayashi, *Nat. Neurosci.* 7, 1104 (**2004**).
9. K. Takao, K. I. Okamoto, T. Nakagawa, R. L. Neve, T. Nagai, A. Miyawaki, T. Hashikawa, S. Kobayashi, and Y. Hayashi, *J. Neurosci.* 25, 3107 (**2005**).
10. H. B. Sun, S. Matsuo, and H. Misawa, *Appl. Phys. Lett.* 74, 786 (**1999**).
11. H. S. Nalwa, Handbook of Organic Conductive Molecules and Polymers, John Wiley, Chichester (**1997**).
12. T. A. Skotheim, R. L. Elsembaumer, and J. R. Reynolds, Handbook of Conducting Polymers, 2nd edn., Marcel Dekker, New York (**1997**).
13. T. A. Skotheim and J. R. Reynolds, Handbook of Conducting Polymers, 3rd edn., CRC Press, Boca Raton, Florida (**2007**).
14. S. Hotta, Electronic and Optical Properties of Conjugated Molecular Systems in Conjugated Phases, Research Signopost, Kerala (**2003**).
15. H. Fukumoto, A. Kumagai, Y. Fujiwara, H. Koinuma, and T. Yamamoto, *Heterocycles* 68, 1349 (**2006**).
16. T. Yasuda, Y. Sasaki, S. Aramaki, and T. Yamamoto, *Chem. Mater.* 17, 6060 (**2005**).
17. W. H. Melhuish, *J. Phys. Chem.* 64, 762 (**1960**).
18. M. A. Albota, C. Xu, and W. W. Webb, *Appl. Optics* 37, 7352 (**1998**).

Received: 28 December 2007. Accepted: 15 February 2008.

COMMUNICATION

CELL STRUCTURE AND FUNCTION 33: 133–141 (2008)

A Mercury Arc Lamp-Based Multi-Color Confocal Real Time Imaging System for Cellular Structure and Function

Kenta Saito[1], Kentaro Kobayashi[1], Tomomi Tani[2], and Takeharu Nagai[1,2]*

[1]Nikon imaging center, Research Institute for Electronic Science, Hokkaido University, N20 W10 Kita-ku, Sapporo, Hokkaido, 001-0020, Japan, and [2]Laboratory for Nanosystems Physiology, Research Institute for Electronic Science, Hokkaido University, N20 W10 Kita-ku, Sapporo, Hokkaido, 001-0020, Japan

ABSTRACT. **Multi-point scanning confocal microscopy using a Nipkow disk enables the acquisition of fluorescent images with high spatial and temporal resolutions. Like other single-point scanning confocal systems that use Galvano meter mirrors, a commercially available Nipkow spinning disk confocal unit, Yokogawa CSU10, requires lasers as the excitation light source. The choice of fluorescent dyes is strongly restricted, however, because only a limited number of laser lines can be introduced into a single confocal system. To overcome this problem, we developed an illumination system in which light from a mercury arc lamp is scrambled to make homogeneous light by passing it through a multi-mode optical fiber. This illumination system provides incoherent light with continuous wavelengths, enabling the observation of a wide range of fluorophores. Using this optical system, we demonstrate both the high-speed imaging (up to 100 Hz) of intracellular Ca^{2+} propagation, and the multi-color imaging of Ca^{2+} and PKC-γ dynamics in living cells.**

Key words: confocal microscopy/live imaging/laser/arc lamp/Nipkow disk

Introduction

Laser-scanning confocal microscopy has been a method of choice for examining biological structures at the sub-cellular, cellular, and tissue levels in three dimensions for several decades, due to its ability to acquire images of thin optical sections within thick samples (Swedlow *et al.*, 2004; Hibbs, 2004). However, a single-point scanning system usually takes several seconds to scan a single viewing field, which is a disadvantage for real-time imaging. Thus, multi-point scanning confocal systems using a scanning disk have been developed to achieve high-speed imaging without losing spatial resolution (Ichihara *et al.*, 1996). The Yokogawa CSU10 is well known as one of the most advanced scanning disk systems. In this system, an expanded laser beam is directed onto a Nipkow disk, which contains arrays made up of tandem pairs of microlenses and pinholes, arranged circumferentially at a constant angle and radially at constantly decreasing distances from the center. When the disk is spun, each microlens/pinhole pair sweeps the excitation laser beam across the object through the objective lens, producing a raster scan of multiple laser beams. This scanning system provides two advantages for confocal imaging: 1) a faster frame acquisition rate (up to 360 Hz) because of the simultaneous scanning by approximately 1200 points, and 2) a reduction of photo-induced damage, because the excitation light power of each scanning point can be reduced to as low as 1/1200 of that of the single-point scanning system (Inoué and Inoué, 2002; Wang *et al.*, 2005). There are some other commercially available disk-scanning systems with pinholes/slits, but they are different from the Yokogawa CSU10. The Olympus DSU employs a scanning disk with silts, which allows the acquisition of quasi-confocal images; however, there is no confocal effect along the horizontal aperture of the slit. The CARV II (BD Bioscience) has a Nipkow disk with pinholes, but the pinholes are larger (CARV II; 70 mm, CSU10; 50 mm), which reduces the confocal effect. Therefore, the axial resolution for both of these systems is lower than for the CSU10 (Toomre and Pawley, 2006).

As the excitation light source, visible wavelength lasers (Argon ion, Krypton-argon ion, Helium-neon ion, and other

*To whom correspondence should be addressed: Takeharu Nagai, Laboratory for Nanosystems Physiology, Research Institute for Electronic Science, Hokkaido University, N20 W10 Kita-ku, Sapporo, Hokkaido, 001-0020, Japan.
Tel: +81-11-706-9438, Fax: +81-11-706-9443
E-mail: tnagai@es.hokudai.ac.jp

Abbreviations: FWHM, Full-width at the half-maximal intensity; OGB, Oregon Green-488 BAPTA-1: PKC-γ, protein kinase C-γ; YC3.60, yellow cameleon 3.60.

solid-state visible lasers) have been used for both single-point and multiple-point scanning confocal systems. However, the use of lasers often limits the choice of fluorescent dyes to be excited, because irradiated laser lights contain a relatively narrow range of wavelengths. Moreover, the use of coherent laser light with a Nipkow-disk confocal system generally results in considerable degradation of the image (Fewer *et al.*, 1998). In contrast to a laser light source, a mercury arc lamp provides incoherent light with a much broader range of wavelengths, from 250 nm to 600 nm, and is commonly used as an excitation light source for conventional wide-field fluorescent microscopes. At a certain wavelength, the axial or lateral resolution of a confocal microscope is determined primarily by the size of the pinhole and the performance of the objective and tube lenses. Thus, confocal-based optical sectioning is possible, regardless of the excitation light source. Based on the idea that the mercury arc lamp provides a much broader range of wavelengths than a laser, illumination with a mercury arc lamp would be preferable for a Nipkow disk confocal system. In spite of this, there has been no report of applying a mercury arc lamp as the light source for the Yokogawa CSU system, possibly due to the difficulty of obtaining intense and uniform illumination of the specimen.

Here we report a method for multiple-point scanning confocal microscopy using a 100 W mercury arc lamp as the light source. In this system, a large diameter (~1 mm in diameter) multi-mode optical fiber is inserted between the arc lamp and the confocal system, providing stable, intense, and uniform illumination. The excitation wavelength is determined by filter selection, as in conventional wide field epi-fluorescence microscopy systems. This microscopy system enables the visualization of multiple-molecular dynamics in living cells without limiting the choice of fluorophores. Using this system, we show both high-speed (up to 100 Hz) and multiple color confocal imaging of dynamic biological events. In addition, we discuss other suitable applications for this new, convenient confocal system.

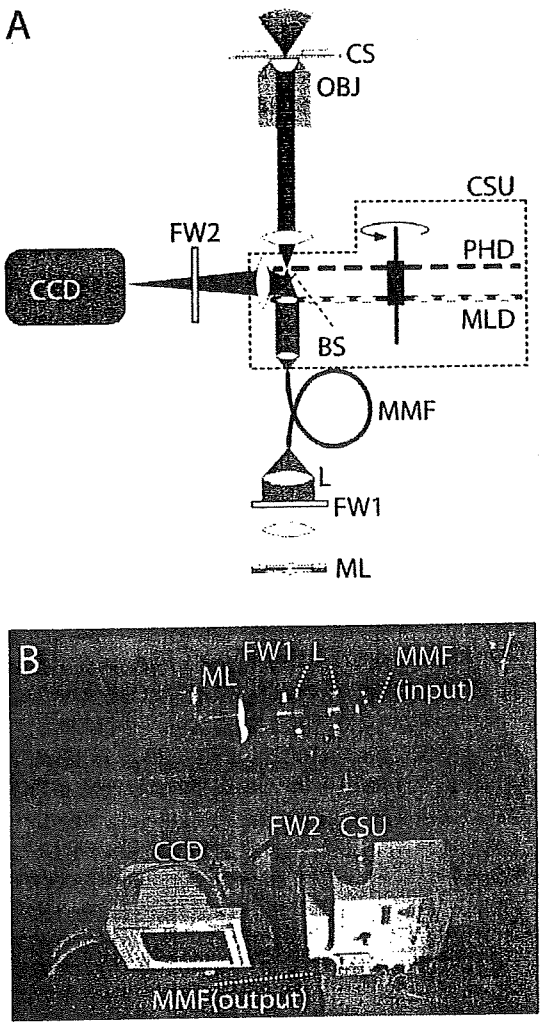

Fig. 1. Nipkow disk confocal unit with mercury arc lamp illumination system. (A) A schematic diagram of the Nipkow disk confocal unit with mercury arc lamp illumination system. ML: 100 W mercury arc lamp, FW1: Filter wheel for excitation, L: collection lens, MMF: multi-mode optical fiber, BS: beam splitter, CSU: Yokogawa CSU10, MLD: microlens array Nipkow disk, PHD: pinhole array Nipkow disk, OBJ: objective lens, CS: cover slip and sample, FW2: filter wheel for emission, CCD: cooled CCD camera. (B) Photograph of the Nipkow disk confocal unit with mercury arc lamp illumination system.

Materials and Methods

Nipkow disk confocal unit with mercury arc lamp illumination system

Fig. 1 shows a schematic diagram of the Nipkow disk confocal unit with a mercury arc lamp illumination system. The system consists of an inverted microscope (TE2000-E, Nikon, Tokyo, Japan) and a commercially available Nipkow disk confocal unit (CSU10, Yokogawa Electric, Tokyo, Japan). A 60×, or 100× PlanApo NA1.4 oil-immersion objective lens (Nikon, Tokyo, Japan) was used to collect the images. The light from a 100 W mercury arc lamp was focused onto the input end (1.0 mm in diameter) of a multi-mode optical fiber (ST1000H; Mitsubishi Electric Cable, Tokyo, Japan) to scramble the light (Kam *et al.*, 1993; Tani *et al.*, 2005). The light from the fiber's output end was then directed to the CSU10. A MAC 5000 system (Ludl, Hawthorne, NY) was used to control the filter wheels for the excitation and emission light and for shuttering the excitation light. The emitted light collected by the objective lens was focused on a cooled electron-multiplying charge-coupled device (EM-CCD) camera (ImagEM; Hamamatsu Photonics, Hamamatsu, Japan) or a cooled 3CCD camera (ORCA-3CCD; Hamamatsu Photonics). The shutter, filter

wheels, and camera were controlled by the software, AquaCosmos version 2.6 (Hamamatsu Photonics).

Spatial resolution measurements

To compare the spatial resolution of a confocal system using a mercury arc lamp with that using an Ar^+ laser, 0.1 μm-diameter fluorescent beads (TetraSpeck; Molecular Probes, Eugene, OR) were used. Excitation light through a mercury arc lamp with a 470/40 nm excitation filter or a 488-nm Ar^+ laser (20 mW; model 532-BS-A04; Melles Griot, Carlsbad, CA) was used to collect images of the beads. Six images obtained using each excitation light were averaged and compared.

Cell preparation

HeLa cells were cultured in homemade 35-mm glass-bottomed dishes in Dulbecco's modified Eagle's medium (DMEM; Sigma, St. Louis MO) containing 10% fetal bovine serum (BioWest, Nuaillé, France). The cells were transfected with plasmids using Lipofectamine 2000 (Invitrogen, Carlsbad, CA). The transfected cells were cultured for 1 to 2 days before observation.

Gene construction

The DNA sequence encoding the N-terminal 12 amino acids of cytochrome *c* oxidase subunit IV (CoxIV) was fused to the sequence encoding the N-terminus of mSECFP (Matsuda *et al.*, 2008), to obtain mSECFP-mit, which specifically localizes to the mitochondrial matrix. The nuclear localization signal sequence (NLS) of SV40 large T-antigen was fused to the C-terminus of mRFP1 (Campbell *et al.*, 2002) to obtain mRFP1-nu, which localizes to the nucleus. mSECFP-er was generated by extending the N-terminus of mSECFP with the signal peptide sequence of calreticulin and the C terminus of mSECFP with the ER retention signal sequence KDEL, which localizes to the endoplasmic reticulum. The sequences encoding mSECFP, mSECFP-mit, mRFP1-nu, and mSECFP-er were cloned into the pcDNA3 vector (Invitrogen, Carlsbad, CA). Venus-Actin was generated by replacing the EYFP gene of pEYFP-Actin (Clontech Laboratories, Palo Alto, CA) with the Venus gene (Nagai *et al.*, 2002). The DsRed1 gene of pPKC-γ-DsRed1 (Clontech Laboratories) was replaced with the gene for its rapidly maturating variant, DsRed T3 (Bevis and Benjamin, 2002) to construct PKC-γ-DsRed T3. The construction of yellow cameleon 3.60 (YC3.60) was reported previously (Nagai *et al.*, 2004).

High-speed [Ca^{2+}] imaging

HeLa cells were incubated in DMEM containing 5 μM Oregon Green-488 BAPTA-1 AM (Molecular Probes, Eugene, OR) for 1 hour at room temperature, washed twice with PBS, and transferred to DMEM again before observation. A 470/40 nm filter (Nikon, Tokyo, Japan) was used as the excitation filter. To show the spatial propagation of the Ca^{2+} wave clearly, the obtained images were

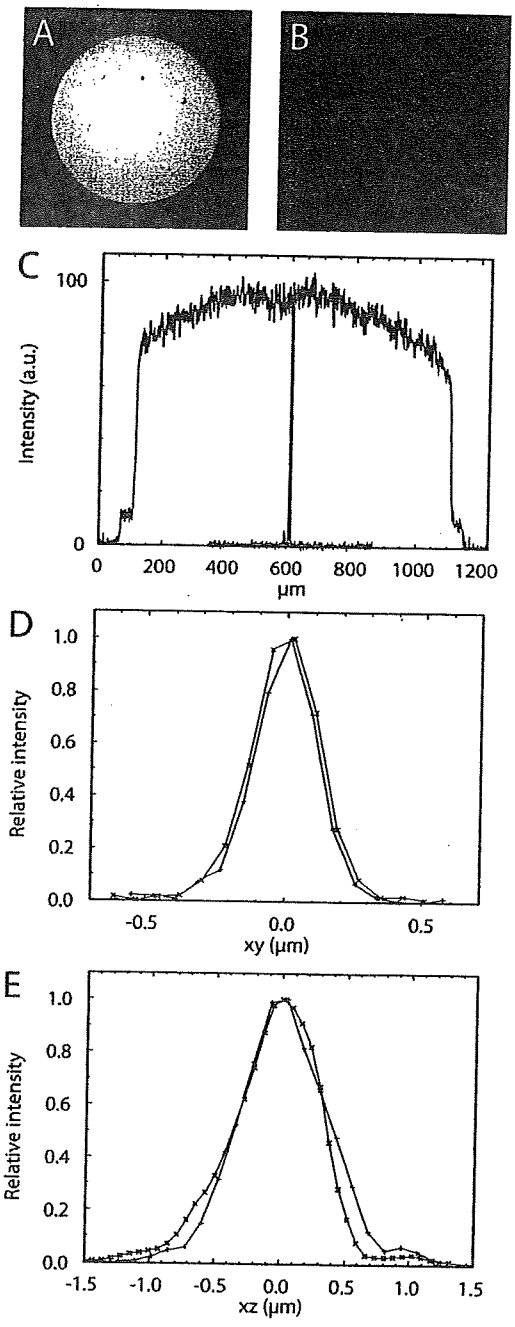

Fig. 2. Comparison of the efficiency of the CSU10 with mercury arc lamp versus 488-nm Ar^+ laser. (A and B) Images of the optical fiber output end coupled to a mercury arc lamp (A) or 488-nm Ar^+ laser (B). (C) The intensity profiles across the center of the images in A (red line) and B (green line), normalized to the peak intensity. (D, E) The spatial resolution of the CSU10 with mercury arc lamp (red line) and 488-nm Ar^+ laser (green line). (D) Horizontal intensity profiles across just the middle section of stacks of a 0.1-μm fluorescent bead. (E) Vertical intensity profiles across the center of a 0.1-μm fluorescent bead.

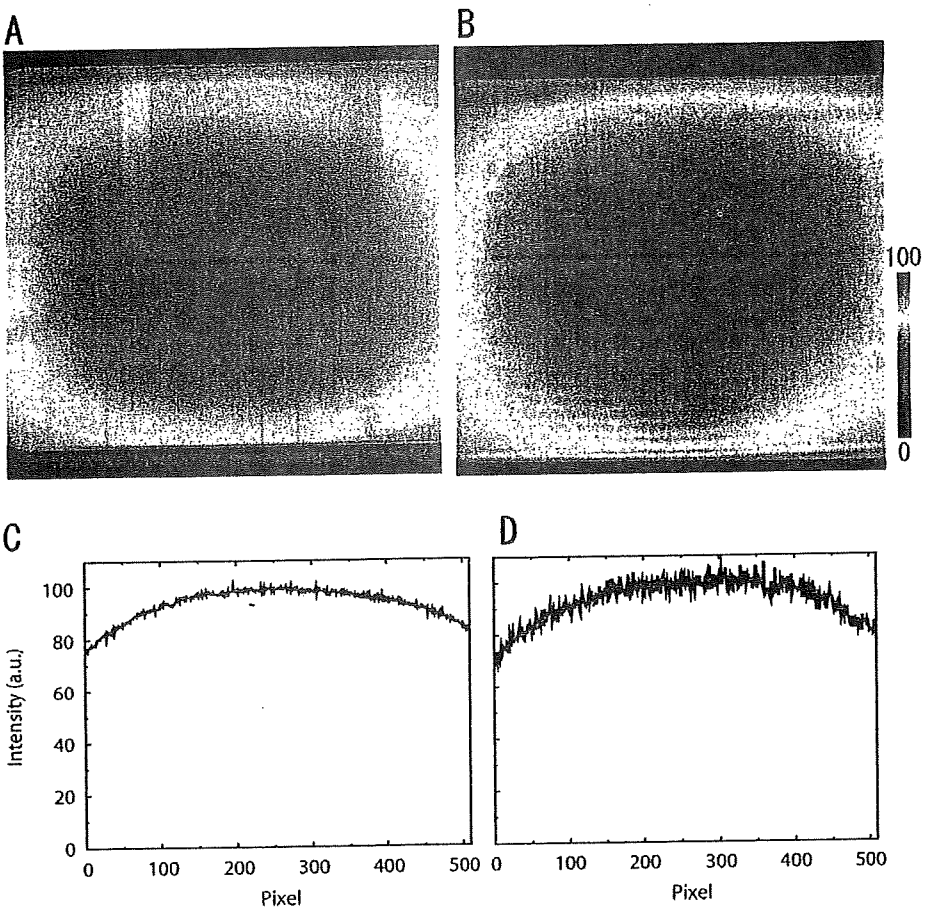

Fig. 3. The uniformity of illumination on a sample. (A and B) The images of a fluorescent plate obtained using the CSU10 with illumination from a mercury arc lamp (A) or 488-nm Ar^+ laser (B). (C and D) The normalized intensity profiles across the center of the images in A (C) and B (D).

smoothed by taking the rolling average over 4 images. From the series of fluorescent images, the relative change in the intracellular Ca^{2+} was calculated from the fluorescence intensity value (F) of the cell divided by its value at time 0 (F_0). The obtained changes in F/F_0 were shown as a series of pseudo-color images.

Multi-color imaging using a half-reflective mirror

For multi-color imaging, we used a half-reflective mirror, T50 (Asahi-spectra Co., Tokyo, Japan), that transmits approximately 50% of visible wavelengths from 400 nm to 700 nm. We used the following combination of excitation and emission filters, respectively: 440/21 nm and 480/30 nm for mSECFP, 490/20 nm and 535/26 nm for Venus, and 540/30 nm and 575 nm long path filter for mRFP1 (all filters were from Omega Optical and are designated by the central wavelengths of their transmittance and band widths at half-maximal transmittance). For the multi-color time-lapse imaging of HeLa cells expressing both YC3.60 and PKC-γ-DsRed T3, we used 440/21 nm and 540/30 nm for YC3.60 and DsRed T3 excitation, respectively, and 480/30 nm, 535/26 nm, and 575 nm long pass filter for mSECFP, Venus, and DsRed T3 emission, respectively. All of the excitation and emission filters were automatically alternated by filter wheels, using the MAC 5000 system (Ludl, Hawthorne, NY).

Results and Discussion

Comparison of illumination at the ends of the optical fiber and spatial resolution using different light sources

A Nipkow disk confocal microscope requires an illumination system that provides uniform excitation light for each scanning point. To obtain uniform illumination from a mercury arc lamp, we introduced a multi-mode, large diameter (1 mm) optical fiber into the illumination system as a light scrambler (Fig. 1A). Typical images of the output end of the multi-mode optical fiber coupled to a mercury arc lamp and

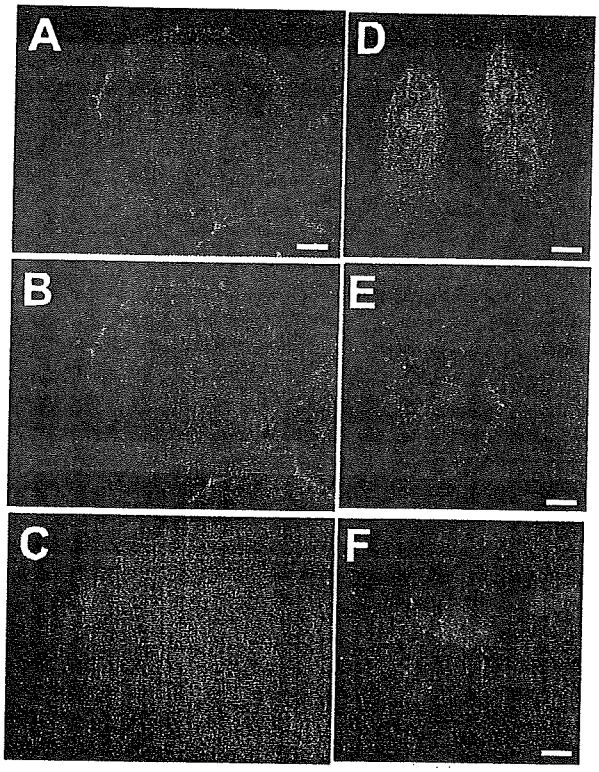

Fig. 4. Optical sectioning of biological samples. (A–C) Real-color images of confocal or non-confocal optical sections of a pumpkin pollen grain. These images were obtained by the CSU10 with a mercury arc lamp (A) or 488-nm Ar^+ laser (B) or by non-confocal (wide field) fluorescence microscopy (C). Scale bar represents 20 μm. (D–F) Images of HeLa cells expressing mSECFP in the cytoplasm and the nucleus (D), mSECFP in the endoplasmic reticulum (E), and mSECFP in the mitochondria (F). Scale bar represents 10 μm.

that of a single-mode optical fiber coupled to a 488-nm Ar^+ laser are shown in Fig. 2A and B, respectively. The intensity profile of the image obtained from the multi-mode fiber output is shown in Fig. 2C. The light was uniformly distributed, and did not reflect the image of the mercury arc's geometry.

The excitation light from the output end of a multi-mode or single-mode fiber end was then introduced into the CSU10 Nipkow disk-type confocal scanner unit. To compare quantitatively the spatial resolution of the system using a mercury arc lamp with that using a 488-nm Ar^+ laser line, we collected three-dimensional images of a 0.1-μm fluorescent bead. The intensity profiles of the images along the X-axis and Z-axis are shown in Fig. 2D and E, respectively. The full width at half-maximal intensity (FWHM) of the images in the xy plane was 0.27 μm for the mercury arc lamp and 0.24 μm for the 488-nm Ar^+ laser (Fig. 2D). The FWHM of the bead image on the xz plane was 0.76 μm for the mercury arc lamp and 0.72 μm for the laser light (Fig. 2E). These results indicate no significant differences in the point-spread function on the xy and xz planes between a CSU10 disk illuminated with a mercury arc lamp versus a 488-nm Ar^+ laser. Thus, the mercury arc lamp illumination was equivalent to the 488-nm Ar^+ laser for acquiring confocal images through the CSU10.

The power and uniformity of illumination

We measured the power of the excitation light of the mercury arc lamp at the input and output ends of the multi-mode optical fiber and at the level of the specimen. With a 470/40 nm band-pass filter, the power at these levels was 60, 8, and 0.05 mW, and with a 540/30 nm band-pass filter, it was 150, 30, and 0.19 mW, respectively. The power of the excitation light with the 470/40 nm filter was lower than that with the 540/30 nm filter, because the mercury arc lamp has prominent emission lines in 540/30 nm but not in 470/40 nm. The applicability of excitation light with no prominent emission line to high-speed imaging will be examined later in this article.

To examine the uniformity of illumination on the specimen, we obtained an image of a fluorescent plate filled with uniformly distributed fluorescent dyes. With both the mercury arc lamp (Fig. 3A) and the 488-nm Ar^+ laser light (Fig. 3B), the peak of intensity was at the center of the image, and about a 20% decrease in signal was seen at the periphery of the image (Fig. 3C, D). In spite of the large difference in the intensity profile at the end of the optical fiber (Fig. 2A–C), there was no significant difference in the uniformity of illumination on the specimen between the mercury arc lamp and the 488-nm Ar^+ laser.

Optical sectioning of biological samples

For further demonstration of the use of the mercury arc lamp as an ideal light source for CSU10, we took confocal fluorescent images of pumpkin pollen grains (diameter, ~100 μm), a useful sample for testing the effect of optical sectioning by confocal systems using a mercury arc lamp (Fig. 4A) and 488-nm Ar^+ laser (Fig. 4B). As a comparison, the same image was taken with a wide-field microscope (Fig. 4C). There was no significant difference between the images obtained using the mercury arc lamp versus the laser (Fig. 4A, B) whereas in the image taken by wide-field microscopy, the inside structure of the pumpkin pollen grain was unclear and the background fluorescence was higher (Fig. 4C) than in the confocal images. Thus, it was fully expected that optical sections of even a single living HeLa cell (~10 μm thickness) might be obtained with the CSU10 with mercury arc lamp system. To verify this, we visualized mSECFP localized to specific organelles in HeLa cells using the CSU10 with a mercury arc lamp as a light source. The condensed structures (vesicles, nucleolus) inside the cell contrasted well with the mSECFP in the cytoplasm and

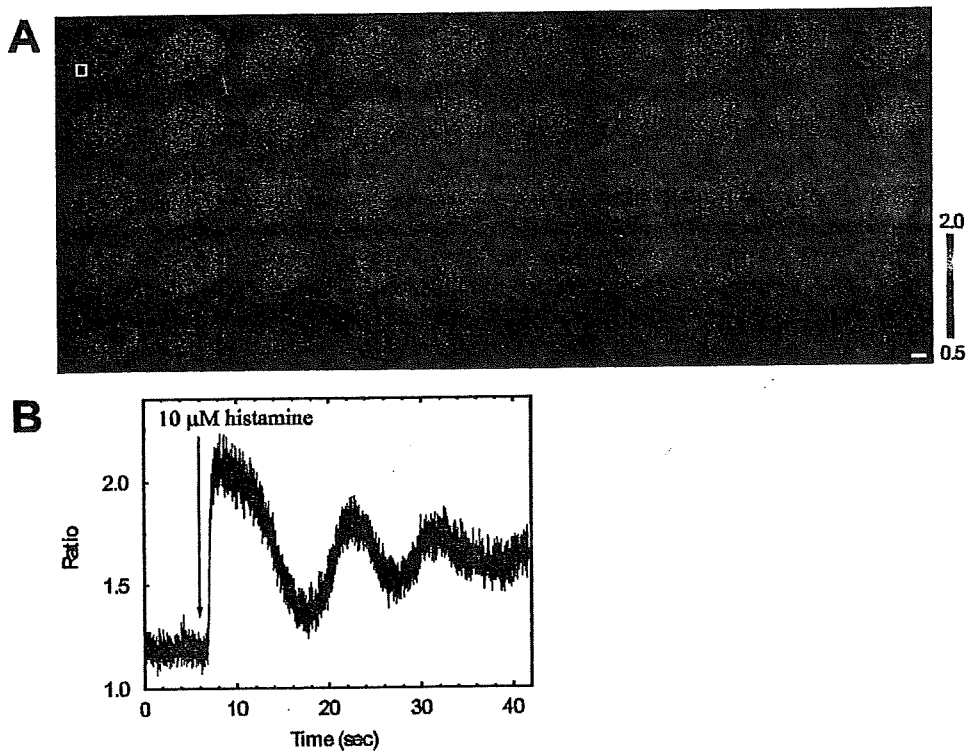

Fig. 5. High-speed confocal Ca^{2+} imaging by the CSU10 with mercury arc lamp. (A) A series of pseudo-colored images of HeLa cells loaded with Oregon Green-488 BAPTA-1 AM. Scale bar represents 10 μm. (B) Time course of the F/F_0 ratio value at the ROI indicated in (A).

the nucleus (Fig. 4D), and the network structure of the endoplasmic reticulum (Fig. 4E), and the tubule structure of the mitochondria (Fig. 4F) were clearly seen. In wide-field microscopy, these structures cannot be seen clearly because of high background fluorescence from the out-of-focus planes.

High-speed confocal imaging with excitation illumination by mercury arc lamp

The mercury arc lamp has several prominent emission lines, at 366, 405, 435, 546, and 578 nm, with peak intensities up to 6–10 times higher than the average intensity of the residual emission wavelength. These prominent emission lines can be used to easily excite fluorescent dyes such as DAPI, CFP, DsRed, and mRFP1 effectively. However, there are no prominent emission lines between 450 nm and 500 nm, which would be applicable to the excitation of various useful fluorescent probes, such as organic compound dyes, Alexa 488, the calcium ion indicator Oregon Green-488 BAPTA-1 (OGB), and the fluorescent proteins EGFP and EYFP. To test the applicability of the CSU10 system with a mercury arc lamp to the fluorescent confocal imaging of dyes that are excited by light from 450 nm to 500 nm, we examined the intracellular Ca^{2+} propagation in HeLa cells using OGB, with a sampling rate of 100 Hz. The fluorescence of OGB loaded into HeLa cells was uniformly distributed in the cytoplasm and the nucleus. After the application of 10 μM histamine (~6 sec after the start of the observation), an increase in Ca^{2+} concentration occurred at the cell periphery that rapidly propagated to the center of the cell (Fig. 5A). The time course of the change in F/F_0 ratio measured in the area enclosed by a white rectangle in Fig. 5B shows an oscillation of intracellular Ca^{2+} concentration with a frequency of approximately 0.1 Hz. This result showed that even at a wavelength of around 500 nm, where no prominent emission lines exist, the CSU10 with a mercury arc lamp could be used to visualize spatial and temporal intracellular Ca^{2+} changes with a time resolution of up to 100 Hz, the same resolution obtained with the CSU10 and a laser light source (Genka *et al.*, 1999).

Multi-color imaging with a half reflective mirror

The wider range of excitation wavelengths emitted by the mercury arc lamp (from 400 nm to 600 nm) allows the visualization of multiple fluorescent dyes. For multi-color imaging with the CSU10, a special interference mirror with multiple transference/reflection peaks (multi-chroic mirror) has been used (Fig. 6A). Since the multi-chroic mirror is

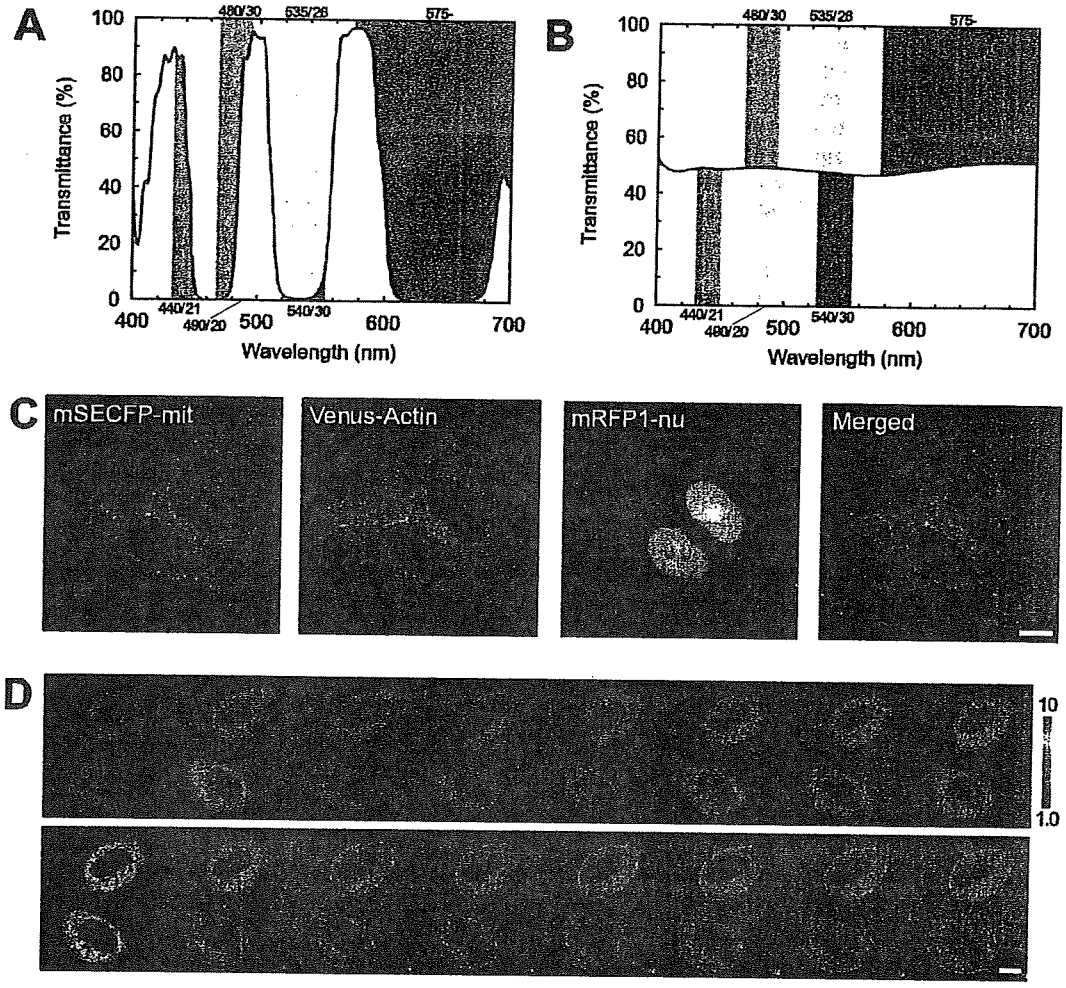

Fig. 6. Multi-color imaging by the CSU10 with a half-reflective mirror. (A) Transmittance of a multi-chroic mirror optimized for three fluorescent proteins: ECFP, EYFP, and mRFP1. (B) Transmittance of the half-reflective mirror, which has about 50% transmittance in the 400–700 nm wavelength range. Areas filled with blue, yellow, or red indicate the amount of light transmitted/reflected by the mirrors and excitation filters and emission filters for ECFP, EYFP, and mRFP1. (C) Images of HeLa cells co-expressing mSECFP-mit, Venus-Actin, and mRFP1-nu. The merged image shows all three channels: green (mSECFP-mit), red (Venus-Actin), and blue (mRFP1-nu). (D) A series of pseudo-colored images of HeLa cells co-expressing YC3.60 (upper panel) and a series of fluorescent images of PKC-γ-DsRed T3 (lower panel). Scale bars in C and D represent 10 μm.

optimized only for cyan, yellow, and red fluorescent dyes, it could limit the advantage of the mercury arc lamp system in providing a broad range of wavelengths. Therefore, to achieve multi-color imaging with the CSU10 with a mercury arc lamp, we introduced a half-reflective mirror instead of the multi-chroic mirror. The transmittance spectrum of the half-reflective mirror is shown in Fig. 6B. Transmission was kept constant at approximately 50% in the 400–700 nm range of the spectrum. By using multiple combinations of excitation and emission filters, multiple images of different colors could be obtained. To compare the transmission/reflection characteristics of the two mirrors described above, the amount of light transmitted/reflected by the mirrors was expressed as areas filled with blue, yellow, and red, if the incident light was an ideal white light (i.e., if the light intensity-wavelength profile were flat). Approximately 50% of the transmitted light through the excitation filter was available for the excitation, and approximately 50% of the collected light through the objective lens could be used for signal detection. The amounts of excitation and emission light in the system using the half reflective mirror were slightly lower than obtained using the multi-chroic mirror. However, the half-reflective mirror should be a powerful choice if one needs to use various combinations of fluorescent dyes for multi-color imaging. To demonstrate the validity of using the half-reflective mirror, we transfected

HeLa cells with the genes for chimeric fluorescent proteins designed to stain different subcellular structures: mitochondria (mSECFP-mit), actin (Venus-Actin), and the nucleus (mRFP1-nu). The HeLa cells were then observed using the CSU10 system with a mercury arc lamp and a half-reflective mirror (Fig. 6C). The three emission signals from the different fluorescent proteins were precisely separated from each other and merged. As shown in Fig. 6C, the three images were well aligned spatially.

We next demonstrated time-lapse imaging of three different colors using the same microscopy system. To monitor the translocation of protein kinase C gamma (PKC-γ) and its upstream Ca^{2+} signal in a living cell, DsRed T3 fused with PKC-γ (PKC-γ-DsRed T3) and yellow cameleon 3.60 (YC3.60) were co-expressed in HeLa cells. YC3.60 is a genetically encoded Ca^{2+} indicator that changes the ratio of YFP and CFP intensity by nearly 600%, based on FRET technology (Nagai *et al.*, 2004). PKC-γ is an isozyme of conventional PKC (cPKC) and has functional C1 and C2 domains in its regulatory region, which bind diacylglycerol and Ca^{2+}, respectively (Nishikawa *et al.*, 1997). Ca^{2+}-mediated PKC-γ activation and translocation to the plasma membrane are well studied (Sakai *et al.*, 1997). Fig. 6D shows a series of pseudo-colored images of HeLa cells expressing YC3.60 (upper panel) and PKC-γ-DsRed T3 (lower panel). The PKC-γ translocation to the plasma membrane was precisely synchronized with the increase in cytoplasmic Ca^{2+} concentration after the application of 10 μM histamine. This result agrees with the previously reported Ca^{2+}-controlled transient membrane association of PKC (Violin *et al.*, 2003).

In this paper, we demonstrated the usefulness of multiple-point scanning confocal microscopy using a 100 W mercury arc lamp as a light source. In our new system, the coupling efficiency between the multi-mode optical fiber and the CSU10 was about 0.01, which is lower than that of CARV II (0.05–0.07), another Nipkow disk-scanning confocal system (Toomre and Pawley, 2006). In spite of the low coupling efficiency, the power of the excitation light with no prominent emission lines of the mercury arc lamp was adequate for high-speed Ca^{2+} imaging at 100 Hz (Fig. 5). In addition, using CSU10 with a mercury arc lamp and a half-reflective mirror may solve the problems associated with multi-color imaging using a laser light source, such as the limitation of fluorophore choice. Many variants of fluorescent proteins have been developed and are available (Giepmans *et al.*, 2006). In particular, red to far-red emitting bright fluorescent proteins have emerged (Merzlyak *et al.*, 2007; Shcherbo *et al.*, 2007). In multi-color imaging, these newly developed red fluorescent proteins are anticipated to be good FRET partners for conventional fluorescent proteins, such as ECFP, EGFP, and EYFP. When we use fluorescent protein variants with longer emission wavelengths, we find that a Xenon arc lamp is superior to the mercury arc lamp, owing to the incident wavelengths expanding to the far-red region. In such cases, a Xenon arc lamp can easily replace the mercury arc lamp as the light source in our microscopy system. Thus, this microscopy system should make multi-color imaging readily available to many researchers.

Acknowledgements. We are grateful to R.Y Tsien for the gift of the mRFP1 plasmid, and we would like to thank M. Shimizu and H. Hirukawa (Yokogawa Electric Corporation) and M. Mizuta and K. Toshimitsu (Nikon Corporation) for technical support and advice. This work was partly supported by Grants from Scientific Research on Advanced Medical Technology of the Ministry of Labor, Health and Welfare of Japan, and the Japanese Ministry of Education, Science and Technology.

References

Bevis, B.J. and Benjamin, S.G. 2002. Rapidly maturing variants of the Discosoma red fluorescent protein (DsRed). *Nat. Biotechnol.*, **20**: 83–87.

Campbell, R.E., Tour, O., Palmer, A.E., Steinbach, P.A., Baird, G.S., Zacharias, D.A., and Tsien, R.Y. 2002. A monomeric red fluorescent protein. *Proc. Natl. Acad. Sci. USA*, **99**: 7877–7882.

Fewer, D.T., Hewlett, S.J., and McCabe, E.M. 1998. Laser sources in direct-view-scanning, tandem-scanning, or Nipkow-disk-scanning confocal microscopy. *Applied Optics*, **37**: 380–385.

Genka, A., Ishida, H., Ichimori, K., Hirota, Y., Tanaami, T., and Nakazawa, H. 1999. Visualization of biphasic Ca^{2+} diffusion from cytosol to nucleus in contracting adult rat cardiac myocytes with an ultra-fast confocal imaging system. *Cell Calcium*, **25**: 199–208.

Giepmans, B.N.G., Adams, S.R., Ellisman, M.H., and Tsien R.Y. 2006. The fluorescent toolbox for assessing protein location and function. *Science*, **312**: 217–224.

Hibbs, A. 2004. Chapter 3-Hardware. In *Confocal Microscopy for Biologists* (A. Hibbs, ed.), Kluwer Academic/Plenum Publishers, New York, pp.90–99.

Ichihara, A., Tanaami, T., Isozaki, K., Sugiyama, Y., Kosugi, Y., Mikuriya, K., Abe, M., and Uemura, I. 1996. High-speed confocal fluorescence microscopy using a Nipkow scanner with microlenses — for 3-D imaging of single fluorescence molecule in real time. *Bioimages*, **4**: 57–62.

Inoué, S. and Inoué, T. 2002. Direct-view high-speed confocal scanner: the CSU-10. *Methods Cell Biol.*, **70**: 87–127.

Kam, Z., Jones, M., Chen, H., Agard, D., and Sedat, J. 1993. Design and construction of an optimal illumination system for quantitative wide-field multi-dimensional microscopy. *Bioimaging*, **1**: 71–81.

Matsuda, T., Miyawaki, A., and Nagai, T. 2008. Direct measurement of protein dynamics inside cells using a rationally designed photoconvertible protein. *Nat. Methods*, **5**: 339–345.

Merzlyak, E., Goedhart, J., Shcherbo, D., Bulina, M., Shcheglov, A., Fradkov, A., Gaintzeva, A., Lukyanov, K., Lukyanov, S., Gadella T., and Chudakov, D. 2007. Bright monomeric red fluorescent protein with an extended fluorescence lifetime. *Nat. Methods*, **4**: 555–557.

Nagai, T., Ibata, K., Park, E.S., Kubota, M., Mikoshiba, K., and Miyawaki, A. 2002. A variant of yellow fluorescent protein with fast and efficient maturation for cell-biological applications. *Nat. Biotechnol.*, **20**: 87–90.

Nagai, T., Yamada, S., Tominaga, T., Ichikawa, M., and Miyawaki, A. 2004. Expanded dynamic range of fluorescent indicators for Ca^{2+} by circularly permuted yellow fluorescent proteins. *Proc. Natl. Acad. Sci. USA*, **101**: 10554–10559.

Nishikawa, K., Toker, A., Johannes, F.J., Zhou, S.Y., and Cantley, L.C. 1997. Determination of the specific substrate sequence motifs of protein kinase C isozymes. *J. Biol. Chem.*, **272**: 952–960.

Sakai, N., Sasaki, K., Ikegaki, N., Shirai, Y., Ono Y., and Saito, N. 1997. Direct visualization of the translocation of the gamma-subspecies of

protein kinase C in living cells using fusion proteins with green fluorescent protein. *J. Cell Biol.*, **139**: 1465–1476.

Shcherbo, D., Merzlyak, E., Chepurnykh, T., Fradkov, A., Ermakova, G., Solovieva, E., Lukyanov, K., Bogdanova, E., Zaraisky, A., Lukyanov, S., and Chudakov, D. 2007. Bright far-red fluorescent protein for whole-body imaging. *Nat. Methods*, **4**: 741–746.

Swedlow, J.R., Andrews, P.D., and Platani, M. 2004. Chapter 17-*In vivo* imaging of Mammalian Cells. In Live Cell Imaging, A Laboratory Manual (R. Goldman and D. Spector, eds.). Cold Spring Harbor Laboratory Press, New York, pp.329–343.

Tani, T., Miyamoto, Y., Fujimori, K.E., Taguchi, T., Yanagida, T., Sako, Y., and Harada, Y. 2005. Trafficking of a ligand-receptor complex on the growth cones as an essential step for the uptake of nerve growth factor at the distal end of the axon: A single-molecule analysis. *J. Neurosci.*, **25**: 2181–2191.

Toomre, D. and Pawley, J. 2006. Disk-Scanning Confocal Microscopy. In *Handbook of biological Confocal Microscopy* (J. Pawley, ed.), SpringerScience+Business Media, New York, pp.221–238.

Violin, J.D., Zhang, J., Tsien, R.Y., and Newton, A.C. 2003. A genetically encoded fluorescent reporter reveals oscillatory phosphorylation by protein kinase C. *J. Cell Biol.*, **161**: 899–909.

Wang, E., Babbey, C., and Dunn, K. 2005. Performance comparison between the high-speed Yokogawa spinning disc confocal system and single-point scanning confocal systems. *J. Microsc.*, **218**: 148–159.

(Received for publication March 31, 2008 and accepted July 30, 2008)

Journal of Biotechnology 137 (2008) 1–7

Contents lists available at ScienceDirect

Journal of Biotechnology

journal homepage: www.elsevier.com/locate/jbiotec

A high-throughput and single-tube recombination of crude PCR products using a DNA polymerase inhibitor and type IIS restriction enzyme

Ippei Kotera[a], Takeharu Nagai[b,*]

[a] PRESTO, Japan Science and Technology Agency, 4-1-8 Honcho Kawaguchi, Saitama 332-0012, Japan
[b] Laboratory for Nanosystems Physiology, Research Institute for Electronic Science, Hokkaido University, Kita-20 Nishi-10 Kita-ku, Sapporo, Hokkaido 001-0020, Japan

Journal of Biotechnology 137 (2008) 1–7

Contents lists available at ScienceDirect

Journal of Biotechnology

journal homepage: www.elsevier.com/locate/jbiotec

A high-throughput and single-tube recombination of crude PCR products using a DNA polymerase inhibitor and type IIS restriction enzyme

Ippei Kotera [a], Takeharu Nagai [b,*]

[a] PRESTO, Japan Science and Technology Agency, 4-1-8 Honcho Kawaguchi, Saitama 332-0012, Japan
[b] Laboratory for Nanosystems Physiology, Research Institute for Electronic Science, Hokkaido University, Kita-20 Nishi-10 Kita-ku, Sapporo, Hokkaido 001-0020, Japan

ARTICLE INFO

Article history:
Received 31 March 2008
Received in revised form 22 June 2008
Accepted 7 July 2008

Keywords:
DNA manipulations
DNA recombination
DNA cloning
Type IIS restriction endonuclease
High-throughput

ABSTRACT

Type IIS restriction enzymes have been successfully used as "universal" restriction enzymes in DNA manipulations. We took a step further to develop a rapid technique for recombining DNA fragments, fully automatic single-tube recombination (FASTR), which enables multiple-fragment DNA recombination in a single step. Crude PCR products are directly mixed with both type IIS restriction endonuclease and DNA ligase to initiate a spontaneous and one-way recombination reaction. Highly efficient DNA recombination can be achieved by an inhibition of DNA polymerase with aphidicolin and a selective digestion of template DNAs by DpnI, a restriction enzyme to digest hemi-methylated DNA in the reaction solution; thereby the entire procedure takes less than 15 min. Owing to its simplicity, efficiency and rapidity, one-step FASTR can be applied to a wide range of DNA manipulations including those involving high-throughput applications where significant reduction in time and cost is expected.

1. Introduction

There have been various approaches to making cloning simpler or faster: instead of using classical restriction enzymes and DNA ligase, DNA recombination systems from different organisms have been used to manipulate plasmid DNA (Hartley et al., 2000; Liu et al., 1998). These techniques have made some repetitious gene clonings easier, but because they are based on DNA recombination, special sequences must accompany the gene to be cloned and the destination vector. These sequences are not removed during the recombination reaction, which is problematic when one tries to fuse one gene to another with a defined linker sequence. Another problem is that if a destination vector is not available for a certain application, one has to make it through conventional plasmid construction. Thus, recombination-based cloning techniques can lack to some degree the flexibility of classical cloning technology.

Type IIS restriction enzymes digest DNA sequence outside of their recognition sequence (Kleid et al., 1976; Takemori et al., 2002). With recognition sequences on primers, type IIS enzymes can be utilized as a universal restriction enzyme for the cloning of PCR products (Podhajska and Szybalski, 1985). We refocused on this classic enzyme because of its versatility and potential for a fast spontaneous DNA recombination reaction. With an inhibition of residual thermostable DNA polymerase activity and selective digestion of template DNAs, we are now able to recombine multiple DNA fragments directly from crude PCR solution in a single tube within 15 min.

2. Materials and methods

2.1. FASTR reaction

PCR was carried out using a high-fidelity thermostable DNA polymerase, KOD-plus (Toyobo, Osaka, Japan) according to the manufacturer's protocol. Briefly, the reaction buffer contained 1× KOD-plus buffer, 2 mM dNTPs, 25 mM $MgSO_4$, 1 unit of KOD-plus, 25 pmol each of forward/reverse primers, and 50 ng each of template plasmids, in a total volume of 50 μl. The template plasmids for mSECFP (Matsuda et al., 2008) and mVenus (Venus (Nagai et al., 2002) with A206K mutations (Zacharias et al., 2002)) were in a pcDNA3.0 vector (Invitrogen, CA, USA), and mCherry (Shu et al., 2006) was in a plant expression vector. pRSET B vector (Invitrogen, CA, USA) was modified by site-directed mutagenesis to delete an LguI site at nucleotide position 2830. The PCR conditions were as follows: 94 °C/2 min (94 °C/15 s, 60 °C/30 s, 68 °C/90 s), 35 cycles, 68 °C/5 min. One microliter of the PCR solution from each sample was transferred to a mixture containing the following reagents in a total volume of 20 μl: 17 mM Tris–acetate, 25 mM Tris–HCl (pH 7.5), 5 mM $MgCl_2$, 5 mM magnesium acetate, 33 mM potassium acetate, 5 mM ATP, 5 mM DTT, 63 μg/ml BSA, 5 U of LguI

* Corresponding author. Tel.: +81 11 706 3833; fax: +81 11 706 4968.
E-mail address: tnagai@es.hokudai.ac.jp (T. Nagai).

0168-1656/$ – see front matter © 2008 Elsevier B.V. All rights reserved.
doi:10.1016/j.jbiotec.2008.07.1816

(Fermentas, ON, Canada), 400 U of T4 DNA ligase (NEB, MA, USA), 20 U of DpnI (NEB, MA, USA), and 5 mM aphidicolin (Calbiochem, CA, USA). The mixture was incubated without agitation at room temperature for various lengths of time. After incubation, 5 μl of the mixture was used to transform *Escherichia coli* (JM109 DE3, Promega, WI, USA). The sequences of the primers used in the FASTR reaction were as follows: pRSET forward primer: GCTACTGCTCTTCGTGCGCTGGTACCATGGAATTCGAA, pRSET reverse primer: CTGATAGCTCTTCTCACGTACAGATCCCGACCCATTTG, GFP-variants forward primer: GCTAGCTCTTCAGTGATGGTGAGCAAGGGCGA and GFP-variants reverse primer: CTAGGCTCTTCTGCACTTGTACAGCTCGTCCATGC. For multiple-fragment FASTR the following sets of primers were used to amplify the inserts: GFP-variants forward 1: GCTAGCTCTTCAGTGATGGTGAGCAAGGGCGA, GFP-variants reverse 1: CTAGGCTCTTCTACCCTTGTACAGCTCGTCCATGC, GFP-variants forward 2: GCTAGCTCTTCAGGTATGGTGAGCAAGGGCGA, GFP-variants reverse 2: CTAGGCTCTTCTGCACTTGTACAGCTCGTCCATGC.

2.2. Fluorescent colony imaging

For the single-color imaging of mSECFP-expressed *E. coli* colonies, an LAS-1000plus image analyzer (Fujifilm, Tokyo, Japan) was used to take fluorescent images. For multicolor imaging, a hand-made device equipped with a Mercury lamp, interference filters, optical fiber cables, and video CCD camera (WAT-120N, Watec, Yamagata, Japan) was used. The filter combination was as follows: 440/21 excitation and 480/30 emission for mSECFP, 500/24 excitation and 535/26 emission for mVenus and 540/30 excitation and 575LP for mCherry. All images were acquired using ImageJ software. MetaMorph (Molecular Devices, CA, USA) was used for image analysis.

2.3. Determination of FRET efficiency

Venus/T-sapphire fusion protein was mixed with 0.05% trypsin–EDTA (Gibco, CA, USA) in PBS and incubated at 37 °C for 1 h. The samples with and without trypsin were analyzed by F-2500 fluorescence spectrophotometer (Hitachi, Tokyo, Japan). The peak values of the donor protein (T-sapphire) before and after the trypsin treatment were used to calculate the FRET efficiency, according to the following equation:

$$E = 1 - \frac{F_{DA}}{F_A}$$

where E is the FRET efficiency of the donor/acceptor pair, F_{DA} is the fluorescence intensity of the donor in the presence of the acceptor (before trypsin treatment), and F_A is the fluorescence intensity of the donor in the absence of the acceptor (after trypsin treatment).

3. Results

3.1. The concept of the FASTR reaction

The DNA cleavage site of type IIS endonucleases is at a distance from their DNA recognition site, thus these enzymes create DNA overhangs of any nucleotide sequence (Szybalski et al., 1991). This feature is advantageous for DNA manipulation in many ways. In carefully designed plasmid constructions, the DNA recognition site for type IIS enzymes can be removed, allowing the ligated final product to be tolerant of the endonuclease that created the overhangs (Lebedenko et al., 1991). This method is more flexible than those using conventional type II endonucleases, because the joint sequence can be designed freely. Another advantage is that the cleavage site does not have to be palindromic, thus preventing undesired homo-ligation between inserts or vectors. We reasoned that, with these features, it might be possible to have both ligation and endonuclease digestion occur simultaneously in the same tube.

As shown in Fig. 1A, all the terminals of the DNA fragments in FASTR carry cleavage sites for type IIS endonuclease followed by recognition sites for the endonuclease. The recognition sites are always outside of the cleavage sites, so after digestion by type IIS endonuclease, no recognition site remains on the DNA fragment. Because both the endonuclease and the ligase are present in the reaction mixture, equilibrium between digestion and ligation is achieved, as long as the ligated product carries the recognition site for the endonuclease. Once ligation between the designated DNA fragments is completed, there is no more digestion even in the presence of the endonuclease, because of the loss of the recognition site. It is this directional reaction that drives the designated products out of the equilibrium, enabling the recombination reaction in a single step (Fig. 1C). The sequence of the cleavage site is independent of the recognition site, allowing the terminus of each DNA fragment to have a specific sticky end for a specific partner fragment. If a three-nucleotide sticky end is used for FASTR, one can theoretically use 4^3, or 64, specific sticky ends, enabling multiple-fragment ligations (Fig. 1B).

3.2. FASTR reaction using gel-purified DNA fragments

To demonstrate this single-step recombination reaction, we amplified both the insert and vector fragments by PCR using pairs of primers with specific cleavage and recognition sites on each end. The amplified fragments were gel-extracted and mixed with type IIS endonuclease (LguI) and T4 DNA ligase. After 2 h of incubation at room temperature, 5 μl of the reaction mixture was used directly to transform chemically competent *E. coli*. To our surprise, eight samples from eight colonies gave positive results for both single- and double-fragment insertions (Fig. 2A). DNA sequencing confirmed that the sequences of the joint region were exactly as designed, verifying the validity of the FASTR reaction (Fig. 2B).

3.3. FASTR reaction using crude PCR products

Encouraged by the result, we thought it might be possible to recombine crude PCR products in a single step. In our early attempts to use this single-tube method, only few positive colonies were obtained (data not shown). We reasoned that the residual activity of the thermostable DNA polymerase would convert the sticky ends to blunt ends, giving rise to self-ligation of the vector plasmid. If so, a DNA polymerase inhibitor might help to reduce the unwanted self-ligation.

Aphidicolin has been known to inhibit the alpha subtype of DNA polymerase in eukaryotes, as well as some types of archaeal DNA polymerases (Ikegami et al., 1978; Klimczak et al., 1985). The KOD-plus DNA polymerase was derived from archaeal *Pyrococcus kodakaraensis* (Takagi et al., 1997). We therefore hypothesized that aphidicolin could inhibit the residual activity of the KOD-plus DNA polymerase present in the PCR product solution, thus allowing a higher recombination rate in the following FASTR reaction. To test the hypothesis, aphidicolin at a final concentration of 2.5 mM was added to the PCR product solution, and 1 μl each of the insert (cyan fluorescent protein, mSECFP) and vector (pRSET B) with the LguI site mutated) solutions were mixed with LguI restriction endonuclease and T4 DNA ligase. DpnI was also included in the reaction to digest the residual template DNA. After vari-

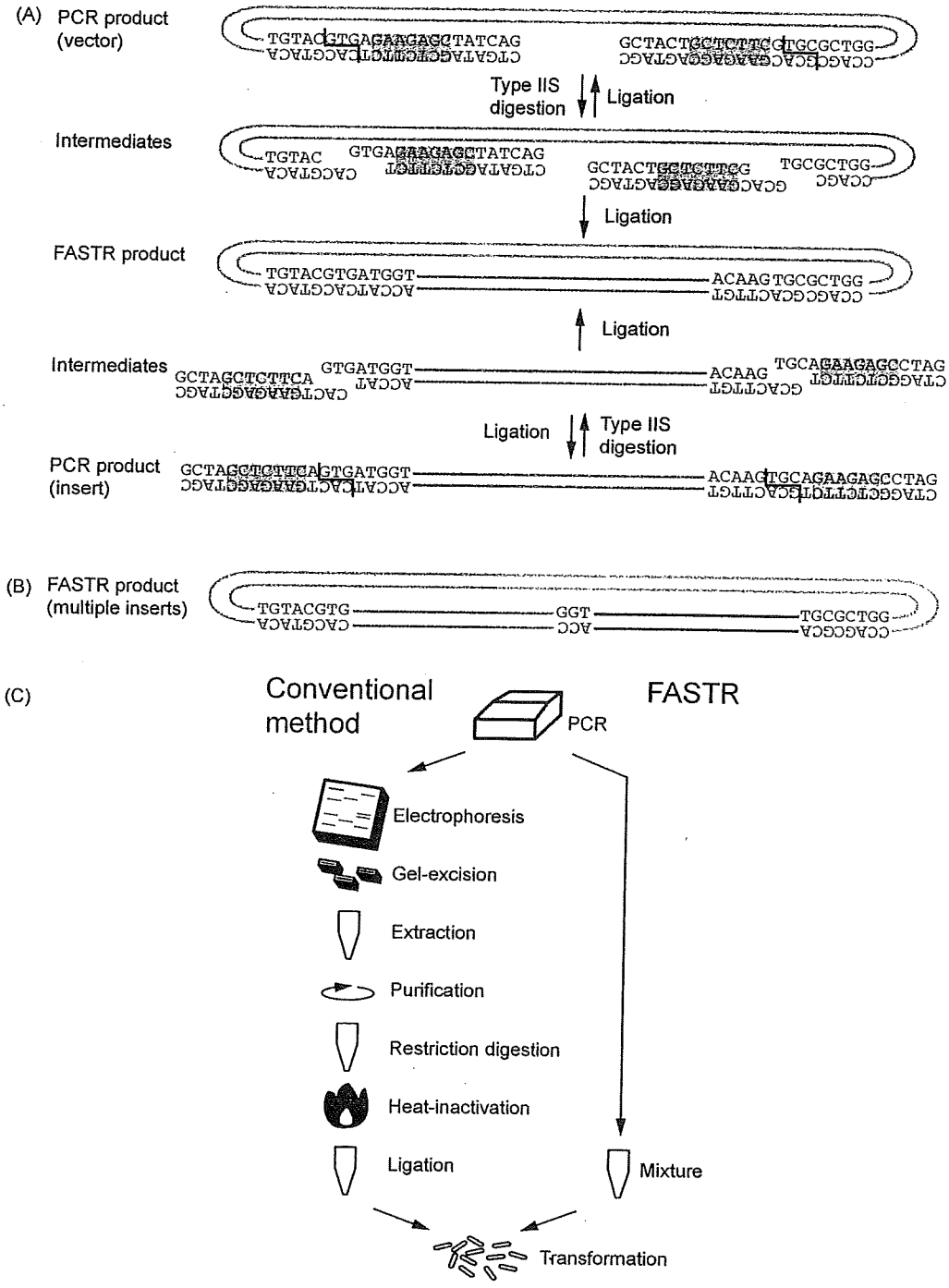

Fig. 1. Schematic representation of the FASTR reactions. (A) PCR products (top and bottom) are treated with both type IIS endonuclease and DNA ligase to induce equilibrium reactions of digestion and ligation. Once the FASTR product is assembled (middle), the reaction stops, because the final product lacks the recognition site for the endonuclease. Blue boxes represent the recognition site for type IIS endonuclease and red lines are the cleavage site of the endonuclease. Vector DNA is in orange and insert DNA is in green. (B) An example of FASTR product with multiple inserts. The inserts are indicated in green and purple. (C) Outline of the FASTR protocol. The entire procedure of FASTR is carried out in a single tube and takes less than 15 min.

ous incubation times at room temperature, JM109 DE3 competent cells were transformed with 5 μl of the FASTR reactant. With 15 min of FASTR reaction at room temperature, more than half of the colonies were fluorescent upon illumination of the plate by 470 nm blue LED. The recombination efficiency reached close to 80% when the incubation time was extended to 2 h (Fig. 2C and D).

3.4. Multiple DNA fragment assembly by FASTR reactions

We next examined the possibility of performing multiple-fragment FASTR with the crude PCR products. The procedures were essentially the same as for single-fragment FASTR, except that the joint sequences were designed so that the insertion fragments would be fused in the correct direction and order

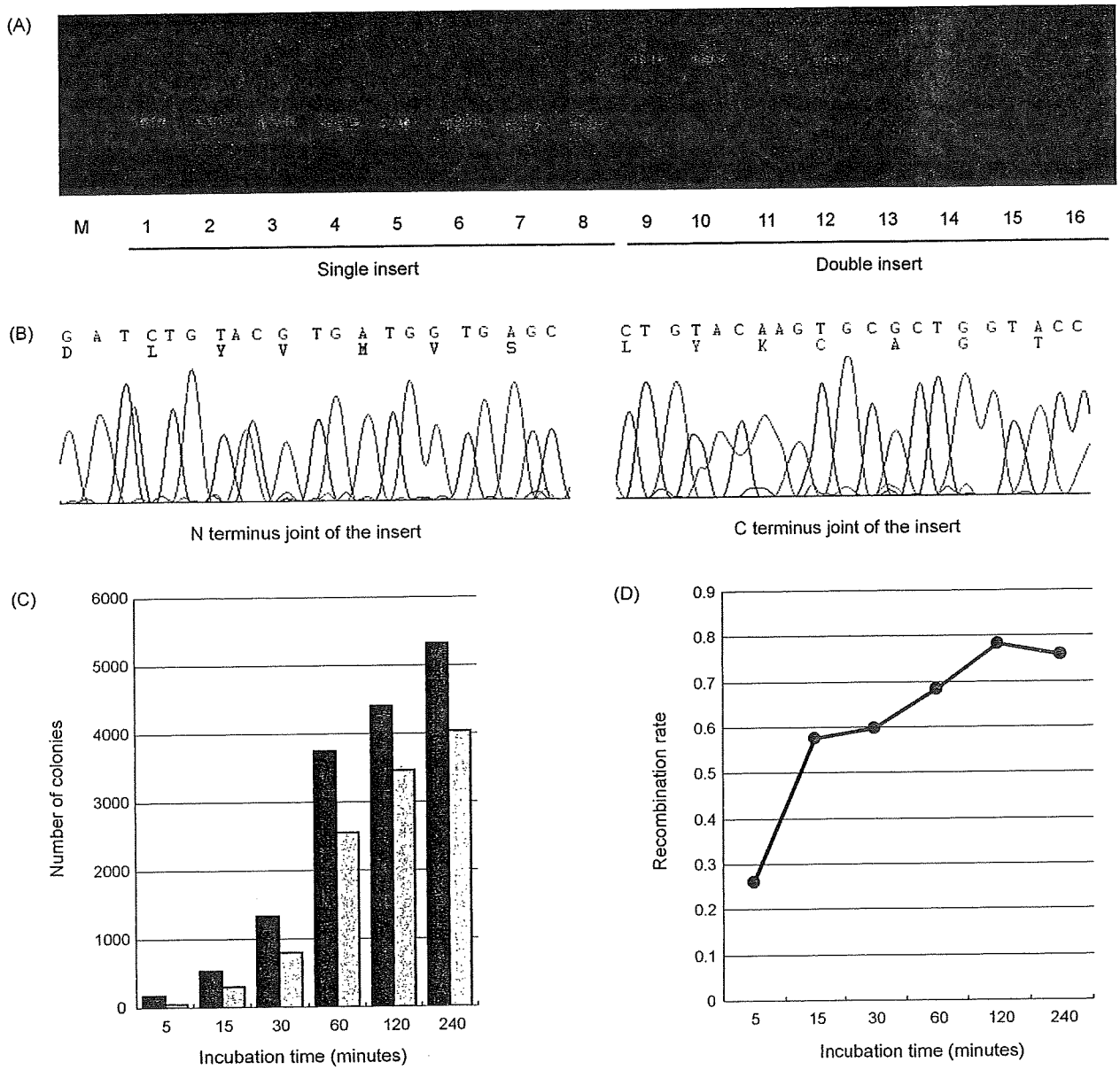

Fig. 2. High recombination rate of FASTR. *E. coli* colonies were obtained by the transformation of FASTR products. The colonies were subjected to colony PCR for insert analysis. (A) Eight randomly picked colonies were positive for single and double insertions. (B) The joints between the vector and insert were DNA sequenced to confirm the validity of the method. The FASTR reaction was carried out for various lengths of time. The number of transformed colonies reached near-plateau at 60 min (C); however, the recombination rate changed little after 15 min (D). Black bars represent the total number of colonies, and gray bars represent the number of fluorescent colonies. The recombination rate was calculated by dividing the number of fluorescent colonies by the total number of colonies.

(Fig. 1B). We amplified the insert fragments of cyan fluorescent protein (mSECFP), yellow fluorescent protein (mVenus), and red fluorescent protein (mCherry) along with the vector fragment of pRSET B. The fragments were then mixed to assemble pRSET–mSECFP–mVenus and pRSET–mSECFP–mVenus–mCherry constructs. The FASTR reaction was performed at room temperature for 1 h. We confirmed that close to half of the fluorescent colonies were double positive for mSECFP and mVenus fluorescence in pRSET–mSECFP–mVenus construct, and around 20% were triple positive for mSECFP, mVenus, and mCherry fluorescence in pRSET–mSECFP–mVenus–mCherry sample (Table 1 and Fig. 3A). These colonies were further analyzed by colony PCR to confirm the inserts (Fig. 3B).

3.5. High-throughput screening of a high-performance FRET probe by FASTR

To demonstrate the feasibility of FASTR in a practical application, we constructed a GFP-based Förster resonance energy transfer

Table 1

Insert	Number of positive colonies	Number of fluorescent colonies	Recombination rate (%)
CFP+Venus	517	1050	49.24
CFP+Venus+mCherry	50	242	20.66

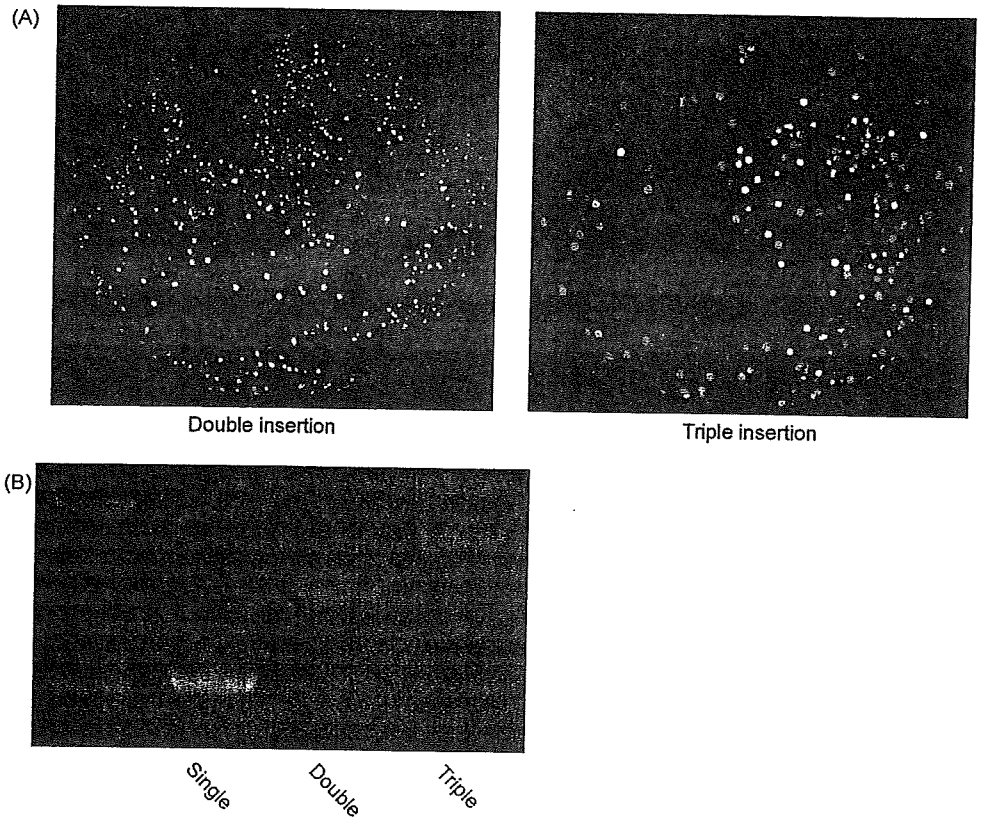

Fig. 3. Double and triple insertion by FASTR. (A) Fluorescent images of colonies expressing mSECFP, Venus, and/or mCherry were taken with multiple filter sets. The images from different color channels were overlaid and pseudocolored. Yellow colonies in the double insertion and white colonies in the triple insertion images are double and triple positives, respectively. (B) Insert lengths of the positive colonies selected by fluorescence were confirmed by colony PCR.

(FRET) pair with various linker regions to maximize FRET efficiency. FRET-based GFP probes have been widely used in biological studies as a genetically encoded molecular sensor (Piston and Kremers, 2007). One obstacle to the technology is that FRET efficiency changes dramatically with very small changes in the distance and relative orientation between fluorophores (Lakowicz, 2006). The sensitivity of a FRET pair is so acute that even a single amino-acid insertion or deletion in the linker region is enough to affect the FRET efficiency. Thus, the construction of a FRET pair requires laborious linker optimization by trial and error (Nagai and Miyawaki, 2004).

Here, we used FASTR to fuse a UV-excitable green fluorescent protein (T-Sapphire) (Zapata-Hommer and Griesbeck, 2003) to Venus, with various linker lengths between them (Fig. 4A). Thirteen reverse primers were designed for C-terminal deletion mutants of Venus, and seven forward primers for N-terminal T-Sapphire deletions. A total of 20 deletion mutants were PCR-amplified. Then 1 μl of the crude PCR products from each sample were mixed in one tube along with FASTR reagents. The FASTR reaction should recombine two inserts and a vector with correct order but in random combinations, giving rise to a total of 91 mutant combinations. After 2 h of incubation at room temperature, JM109 competent cells were transformed with 10 μl of the reactant. *E. coli* plates were screened for yellowish fluorescent colonies using a 405 nm light source. DNA sequencing of the linker region and spectroscopic analysis of the expressed proteins identified the clones with high FRET efficiency (Fig. 4B). The FRET efficiency of the best clone we obtained was determined to be 67% by cleaving the linker region (Fig. 4C), demonstrating that FASTR is an ideal method for creating a large number of multiple-fragment constructs for high-throughput screening.

4. Discussion

Although cloning techniques with type IIS restriction endonucleases and DNA ligases have been widely used, the endonuclease-mediated single-step recombination in our method is much faster than previous approaches. As far as we know, this is the first report which describes the spontaneous and directional single-tube recombination with a type IIS restriction endonuclease and DNA ligase. The reaction allows highly efficient DNA recombination, while keeping a high flexibility of class IIS restriction enzymes. Another advantage of our approach is the ability to directly recombine crude PCR products. This was made possible by adding an archeal DNA polymerase inhibitor to the FASTR reaction. Although we have not tried a monoclonal antibody against the polymerase, it might also be used to inactivate the residual polymerase activity, as it is for hot-start PCR (Kellogg et al., 1994). DpnI was also included in the reaction to selectively digest the bacterially expressed template DNA in the crude PCR products.

We primarily focused our efforts on improving the rapidity of the method, because we thought that raising the speed limit for DNA recombination would enhance research in many fields, especially ones involving high-throughput analysis. One such field is the development of GFP-based FRET probes, which are now indispensable in the biological sciences. A typical FRET probe has fluorescent donor and acceptor domains along with a sensor domain to detect biological signals. High FRET efficiency is achieved only when the distance between fluorophores is comparable to the Förster distance, and the relative dipole moments of the fluorophores are parallel to each other. The distance between fluorophores is largely affected by the linker sequences between

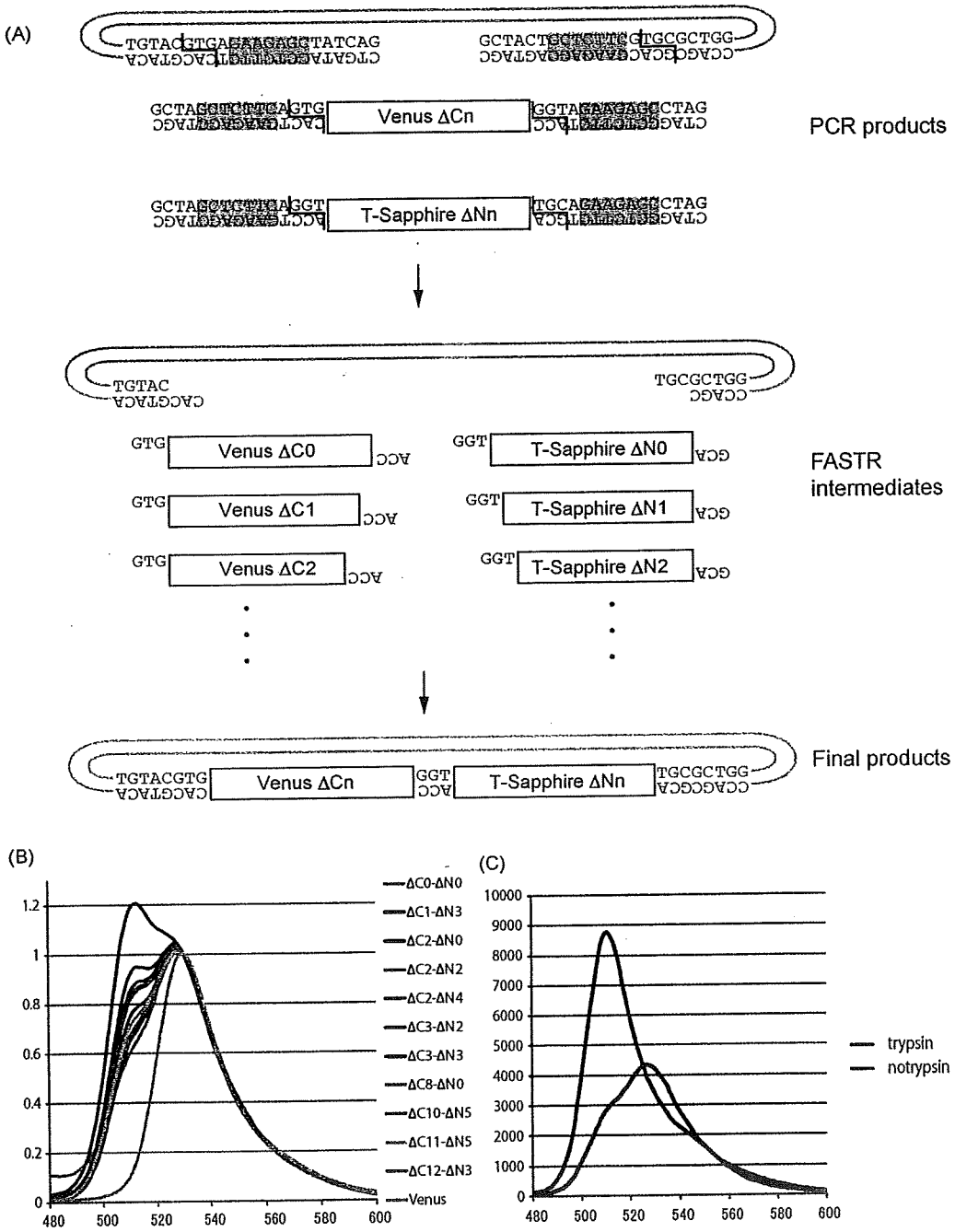

Fig. 4. Optimization of a GFP-based FRET pair. (A) A schematic representation of FRET pair optimization by FASTR. GFP variants with various lengths of linker regions are PCR-amplified (top). FASTR intermediates are indicated in the middle panel. The final products are represented in the bottom panel. An N-terminal deletion is indicated as ΔN1 and a C-terminal deletion as ΔC1. 'n' deletions are represented as ΔNn or ΔCn. (B) Fluorescence spectra of Venus (511 nm) and T-Sapphire (527 nm) fusion proteins with various linker regions. The spectra were obtained by 395 nm illumination and fluorescence scanning with a 5 nm slit. The curves were normalized to the fluorescence intensity at 530 nm. (C) Venus-T-sapphire (ΔC2–ΔN0) fusion protein was cleaved into separate fluorophores by trypsin. The FRET efficiency of the pair was calculated by fluorescence recovery of the donor protein (T-sapphire).

the domains, and the relative orientation of the fluorophores can be changed by using circular permutations of the fluorescent proteins (Nagai et al., 2004). Since it is very difficult to predict the structural state of the fluorophores by calculation, one has to optimize these parameters through empirical methods. FASTR technology can contribute to the development of such probes, because it can assemble multiple domains of FRET probes simultaneously, saving the time and cost of constructing numerous combinations of linkers and domains to obtain a favorable FRET signal.

A possible drawback of FASTR methodology would be the requirement of primers for each FASTR reaction. Although the cost and availability of synthetic oligonucleotides have been greatly improved, the requirement might be an obstacle to some researchers. Another drawback would be the imcompatibility of FASTR products with conventional restriction enzymes; the liga-

tion site of the FASTR products cannot be recut with conventional restriction enzymes. We recommend another round of FASTR reaction for an additional plasmid modification, and colony PCR for insert check.

FASTR technology is among the quickest in the latest generation of recombinant technologies, while it achieves the high efficiency of recombination-based methods and the flexibility of conventional cloning. These advantages should be applicable to most DNA manipulation procedures, including high-throughput DNA manipulations, where significant savings in time and cost are expected.

Acknowledgments

We are thankful to R.Y. Tsien for the gift of mCherry plasmid. We also thank Wataru Tomosugi for the construction of T-Sapphire plasmid, by mutating EGFP plasmid according to the published data. This work was partly supported by grants from Scientific Research on Advanced Medical Technology of the Labor, Health and Welfare of Japan to T.N., the Japanese Ministry of Education, Science and Technology to T.N., and Precursory Research for Embryonic Science and Technology (PRESTO) of the Japan Science and Technology Agency (JST) to I.K.

References

Hartley, J.L., Temple, G.F., Brasch, M.A., 2000. DNA cloning using in vitro site-specific recombination. Genome Res. 10, 1788–1795.

Ikegami, S., Taguchi, T., Ohashi, M., Oguro, M., Nagano, H., Mano, Y., 1978. Aphidicolin prevents mitotic cell division by interfering with the activity of DNA polymerase-alpha. Nature 275, 458–460.

Kellogg, D.E., Rybalkin, I., Chen, S., Mukhamedova, N., Vlasik, T., Siebert, P.D., Chenchik, A., 1994. TaqStart antibody: "hot start" PCR facilitated by a neutralizing monoclonal antibody directed against Taq DNA POLYMERASE. Biotechniques 16, 1134–1137.

Kleid, D., Humayun, Z., Jeffrey, A., Ptashne, M., 1976. Novel properties of a restriction endonuclease isolated from *Haemophilus parahaemolyticus*. Proc. Natl. Acad. Sci. U.S.A. 73, 293–297.

Klimczak, L.J., Grummt, F., Burger, K.J., 1985. Purification and characterization of DNA polymerase from the archaebacterium *Sulfolobus acidocaldarius*. Nucleic Acids Res. 13, 5269–5282.

Lakowicz, J.R., 2006. Principles of Fluorescence Spectroscopy. Springer, New York, pp. 443–475.

Lebedenko, E.N., Birikh, K.R., Plutalov, O.V., Berlin Yu, A., 1991. Method of artificial DNA splicing by directed ligation (SDL). Nucleic Acids Res. 19, 6757–6761.

Liu, Q., Li, M.Z., Leibham, D., Cortez, D., Elledge, S.J., 1998. The univector plasmid-fusion system, a method for rapid construction of recombinant DNA without restriction enzymes. Curr. Biol. 8, 1300–1309.

Matsuda, T., Miyawaki, A., Nagai, T., 2008. Direct measurement of protein dynamics inside cells using a rationally designed photoconvertible protein. Nat. Methods 5, 339–345.

Nagai, T., Miyawaki, A., 2004. A high-throughput method for development of FRET-based indicators for proteolysis. Biochem. Biophys. Res. Commun. 319, 72–77.

Nagai, T., Ibata, K., Park, E.S., Kubota, M., Mikoshiba, K., Miyawaki, A., 2002. A variant of yellow fluorescent protein with fast and efficient maturation for cell-biological applications. Nat. Biotechnol. 20, 87–90.

Nagai, T., Yamada, S., Tominaga, T., Ichikawa, M., Miyawaki, A., 2004. Expanded dynamic range of fluorescent indicators for $Ca^{(2+)}$ by circularly permuted yellow fluorescent proteins. Proc. Natl. Acad. Sci. U.S.A. 101, 10554–10559.

Piston, D.W., Kremers, G.J., 2007. Fluorescent protein FRET: the good, the bad and the ugly. Trends Biochem. Sci. 32, 407–414.

Podhajska, A.J., Szybalski, W., 1985. Conversion of the FokI endonuclease to a universal restriction enzyme: cleavage of phage M13mp7 DNA at predetermined sites. Gene 40, 175–182.

Shu, X., Shaner, N.C., Yarbrough, C.A., Tsien, R.Y., Remington, S.J., 2006. Novel chromophores and buried charges control color in mFruits. Biochemistry 45, 9639–9647.

Szybalski, W., Kim, S.C., Hasan, N., Podhajska, A.J., 1991. Class-IIS restriction enzymes—a review. Gene 100, 13–26.

Takagi, M., Nishioka, M., Kakihara, H., Kitabayashi, M., Inoue, H., Kawakami, B., Oka, M., Imanaka, T., 1997. Characterization of DNA polymerase from Pyrococcus sp. strain KOD1 and its application to PCR. Appl. Environ. Microbiol. 63, 4504–4510.

Takemori, H., Katoh, Y., Horike, N., Doi, J., Okamoto, M., 2002. ACTH-induced nucleocytoplasmic translocation of salt-inducible kinase Implication in the protein kinase A-activated gene transcription in mouse adrenocortical tumor cells. J. Biol. Chem. 277, 42334–42343.

Zacharias, D.A., Violin, J.D., Newton, A.C., Tsien, R.Y., 2002. Partitioning of lipid-modified monomeric GFPs into membrane microdomains of live cells. Science 296, 913–916.

Zapata-Hommer, O., Griesbeck, O., 2003. Efficiently folding and circularly permuted variants of the Sapphire mutant of GFP. BMC Biotechnol. 3, 5.

Direct measurement of protein dynamics inside cells using a rationally designed photoconvertible protein

Tomoki Matsuda[1], Atsushi Miyawaki[2] & Takeharu Nagai[1]

All biological reactions depend on the diffusion and re-localization of biomolecules. Our understanding of biological processes requires accurate measurement of biomolecule mobility in living cells. Currently, approaches for investigating the mobility of biomolecules are generally restricted to measuring either fast or slow diffusion kinetics. We describe the development and application of a photoconvertible fluorescent protein, Phamret, that can be highlighted by UV light stimulation inducing a change in fluorescence emission from cyan fluorescent protein (CFP) to photoactivated GFP (PA-GFP). Phamret can be monitored by single excitation-dual emission mode for visualization of molecular dynamics for a broad range of kinetics. We also devised a microscopy-based method to measure the diffusion coefficient from the fluorescence decay after photostimulation of Phamret, enabling analysis of diffusion kinetics ranging from less than 0.1 μm²/s up to ~100 μm²/s, and found significant changes in free protein movement during cell-cycle progression.

Application of GFP and related fluorescent proteins has revolutionized our ability to analyze a wide range of biological processes such as gene expression, protein localization and cell motility in living specimens. Advances in fluorescence microscopy techniques have also enabled higher-resolution imaging of the fluorescence signals from fluorescent protein fusion constructs, providing insights into the movement of biomolecules and their interactions with cellular components[1,2].

Among these methods, imaging fluorescence resonance energy transfer (FRET) between two fluorescent proteins provides spatiotemporal information of protein-protein interactions and protein conformational changes in living cells[3]. FRET is the radiation-less energy transfer from an excited donor to an acceptor fluorophore that occurs when both molecules are in close proximity within ~10 nm at an appropriate orientation of the dipole moment. This technology has been used to develop genetically encoded fluorescent indicators for various cellular events[3].

Several microscopy techniques, including fluorescence correlation spectroscopy (FCS) and fluorescence recovery after photobleaching (FRAP), are used to investigate mobility of biomolecules in living cells. FCS is used to determine the diffusion coefficient and the concentration of biomolecules in live cells by monitoring fluctuations in fluorescence intensity in a diffraction-limited spot of a laser beam[4]. FRAP is also used to investigate protein dynamics by photobleaching fluorescent molecules using a high-powered laser and then recording the movement of surrounding non-bleached fluorescent molecules into the photobleached area[5]. From the recovery curve, it is possible to estimate both the diffusion coefficient and immobile fraction of the tested proteins[6].

In recent years, various photosensitive fluorescent proteins have been developed by engineering existing fluorescent proteins or cloning new proteins from fluorescent organisms[7]. These photosensitive fluorescent proteins provide means to optically highlight selected proteins and to measure protein dynamics. Photosensitive fluorescent proteins can be classified into two types: photoactivatable and photoconvertible fluorescent proteins. Photoactivatable fluorescent proteins are those that are reversibly or irreversibly changed from a dark state to a bright state by photostimulation, such as PA-GFP[8], photoactivatable mRFP1 (ref. 9), KFP1 (ref. 10) and Dronpa[11]. In contrast, photoconvertible fluorescent proteins maintain a bright state but undergo an emission wavelength change from the pre- to post-photoconversion state by photostimulation. Examples of photoconvertible fluorescent proteins are Kaede[12], mEosFP[13], PS-CFP[14], KikGR[15] and Dendra[16]. The ability to detect both pre- and post-photoconversion states is a preferred characteristic for live-cell imaging, but all presently available photoconvertible fluorescent proteins undergo a change in excitation wavelength in addition to the shift in emission wavelength. This therefore requires a complicated microscope setup and also makes it difficult to measure rapid molecular dynamics. Furthermore, photoconvertible fluorescent proteins except PS-CFP, mEosFP and Dendra function as oligomers, which hinders their use as protein tags.

To overcome these problems, we rationally designed a monomeric photoconvertible fluorescent protein, Phamret, that requires only one wavelength to excite both the pre- and post-photoconverted states, thus enabling quantitative observation of rapidly diffusible molecules. We also developed a microscopy method, FDAP, for measurement of rapid diffusion of molecules, up to ~100 μm²/s using Phamret or other photosensitive

[1]Laboratory for Nanosystems Physiology, Research Institute for Electronic Science, Hokkaido University, Kita-12 Nishi-6 Kita-ku, Sapporo, Hokkaido, 060-0812, Japan. [2]Laboratory for Cell Function and Dynamics, Brain Science Institute, RIKEN, 2-1 Hirosawa, Wako, Saitama, 351-0198, Japan. Correspondence should be addressed to T.N. (tnagai@es.hokudai.ac.jp).

RECEIVED 2 JANUARY; ACCEPTED 14 FEBRUARY; PUBLISHED ONLINE 16 MARCH 2008; DOI:10.1038/NMETH.1193